

# Multi-phonon Resonant Raman Scattering Predicted in LaMnO<sub>3</sub> from the Franck-Condon Process *via* Self-Trapped Excitons

Vasili Perebeinos and Philip B. Allen

*Department of Physics and Astronomy, State University of New York, Stony Brook, NY 11794-3800*

(October 27, 2018)

Resonant behavior of the Raman process is predicted when the laser frequency is close to the orbital excitation energy of LaMnO<sub>3</sub> at 2 eV. The incident photon creates a vibrationally excited self-trapped “orbiton” state from the orbitally-ordered Jahn-Teller (JT) ground state. Trapping occurs by local oxygen rearrangement. Then the Franck-Condon mechanism activates multiphonon Raman scattering. The amplitude of the  $n$ -phonon process is first order in the electron-phonon coupling  $g$ . The resonance occurs *via* a dipole forbidden  $d$  to  $d$  transition. We previously suggested that this transition (also seen in optical reflectivity) becomes allowed because of asymmetric oxygen fluctuations. Here we calculate the magnitude of the corresponding matrix element using local spin-density functional theory. This calculation agrees to better than a factor of two with our previous value extracted from experiment. This allows us to calculate the absolute value of the Raman tensor for multiphonon scattering. Observation of this effect would be a direct confirmation of the importance of the JT electron-phonon term and the presence of self-trapped orbital excitons, or “orbitons.”

## I. INTRODUCTION

Manganese oxide materials attract attention because of the “colossal magnetoresistance” (CMR) phenomenon [1], and because of a very rich phase diagram [2] of ground states with competing order parameters. The Mn<sup>+3</sup> ion of the parent LaMnO<sub>3</sub> compound has  $d^4$  ( $t_{2g}^3, e_g^1$ ) configuration with an inert  $t_{2g}$  core (spin 3/2). The half-filled doubly degenerate  $e_g$  orbitals ( $d_{x^2-y^2}$ ,  $d_{3z^2-r^2}$ ) are Jahn-Teller (JT) unstable. A symmetry-breaking oxygen distortion (resulting in the Mn-O bond lengths of 1.91, 2.18 and 1.97 Å [3]) lowers the energy of the occupied orbital. The corresponding orbitally ordered state sets in at  $T_{JT} = 750$  K with  $x$ - and  $y$ -oriented  $e_g$  orbitals in the  $x - y$  plane with wavevector  $\vec{Q} = (\pi, \pi, 0)$  [4]. The orbital order drives antiferromagnetic ( $A$ -type) spin order [5] below the Neel temperature  $T_N = 140$  K.

There is still controversy about the origin of the orbitally ordered state. Strong electron-electron correlations may lead to orbital order *via* the superexchange interaction [6] which lifts degeneracy of the  $e_g$  states [7]. In another scenario proposed by Millis [8] the Jahn-Teller electron-phonon (e-ph) interaction  $g$  [9] causes the orbital order and contributes to CMR. Extensive numerical work by Dagotto *et al.* [10] showed that the two approaches give qualitatively similar answers. We prefer a model where the JT interaction  $g$  plus large Hubbard  $U$  and Hund energy  $J_H$  leads to single occupancy of the Mn  $e_g$  levels and a gap to on-site  $d$  to  $d$  excitations, rather than assigning the gap purely to Coulomb interactions as in a multi-orbital Hubbard model. We believe that the importance of the JT interaction is evident at low hole doping of La<sub>1-x</sub>Sr(Ca)<sub>x</sub>MnO<sub>3</sub>, whose insulating nature is naturally explained by formation of the anti-Jahn-Teller polarons [11].

In this paper we present a detailed prediction of resonant multiphonon Raman features, whose observation would be a direct measure of the importance of the JT electron-phonon term. When the oscillator potential curves of ground and excited states are displaced relative to each other, then vibrational Raman scattering is activated by a Franck-Condon (FC) two-step mechanism. Our Hamiltonian for LaMnO<sub>3</sub>, with  $U \rightarrow \infty$ , leads to a picture where the ground state and low-lying excited states are simple products of localized orbitals, one per atom. In the first step of the FC Raman process, the incident photon creates an orbital defect in the ordered JT ground state (one Mn ion has the upper rather than the lower state of the JT doublet occupied.) This Frenkel exciton (also called an “orbiton”) is self-trapped [12] by oxygen rearrangement from the JT state. The FC principle has the oxygen positions undistorted during optical excitation, producing a vibrationally excited state of the orbiton. In the second step of the Raman process, this virtual excitation decays back to the orbital ground state, but not necessarily the vibrational ground state. The amplitude for ending in a vibrationally excited state is determined by displaced-oscillator overlap integrals. This allows  $n$ -phonon resonant Raman scattering with amplitude proportional to the first order of the e-ph interaction [13]. The process is illustrated in Fig. 1. In the conventional Raman scattering process, where electronically excited states do not alter atomic positions, the amplitude of the  $n$ -phonon peak is proportional to the  $n$ th order of the e-ph

interaction which is smaller by  $n - 1$  orders of magnitude. The conventional process can be divided into three steps. (1) The incident photon creates an electron-hole pair (or exciton). (2) This electron-hole pair is scattered into another state by sequential emission of  $n$  phonons *via*  $n$  powers of the e-ph interaction  $\mathcal{H}_{\text{e-ph}} \propto g$ . Higher-order interactions, such as the electron-(two phonon) interaction also enter, but do not increase the order of magnitude of the process. (3) The electron-hole pair recombines, emitting a scattered photon. In this formulation, the intensity of the two-phonon Raman process is smaller than one-phonon by several orders of magnitude  $10^{-2}$ - $10^{-3}$ , determined by the  $2n$ -th power of the ratio of e-ph to electronic energies.

## II. FRANCK-CONDON MECHANISM

We use a model Hamiltonian [11], essentially the same as used by Millis [14], with two  $e_g$  orbitals per Mn atom, fully respecting the symmetries of the orbitals and the crystal. The electron-phonon term  $\mathcal{H}_{\text{JT}}$  stabilizes the orbitally-ordered ground state *via* a cooperative JT distortion. Oxygen displacements along Mn-O-Mn bonds are modeled by local Einstein oscillators:

$$\begin{aligned}\mathcal{H}_{\text{JT}} &= -g \sum_{\ell, \alpha} \hat{n}_{\ell, \alpha} (u_{\ell, \alpha} - u_{\ell, -\alpha}) \\ \mathcal{H}_{\text{L}} &= \sum_{\ell, \alpha} (P_{\ell, \alpha}^2 / 2M + K u_{\ell, \alpha}^2 / 2).\end{aligned}\quad (1)$$

The interaction  $\mathcal{H}_{\text{JT}}$  consists of linear energy reduction of an occupied  $d_{3x^2-r^2}$  orbital (the corresponding creation operator is  $c_x^\dagger$  and number operator is  $\hat{n}_{\ell, x} = c_x^\dagger(\ell)c_x(\ell)$ ) if the two oxygens in the  $\pm \hat{x}$  direction expand outwards. Similar terms are included for  $\hat{y}$  and  $\hat{z}$  oxygens if  $d_{3y^2-r^2}$  or  $d_{3z^2-r^2}$  orbitals are occupied. The strength  $g=1.84$  eV/Å of the JT coupling  $g$  determines the JT splitting of the orbitals  $2\Delta = 1.9$  eV, and was chosen to agree with the lowest optical conductivity peak [15]. The displacement  $u_{\ell, \alpha}$  is measured from the cubic perovskite position of the nearest oxygen in the  $\hat{\alpha}$ -direction to the Mn atom at  $\ell$ . The oxygen vibrational energy  $\hbar\omega = \hbar\sqrt{K/M} = 0.075$  eV is taken from a Raman experiment [16]. In addition there is an on site Coulomb repulsion  $U$  and a large Hund energy  $J_H$ . In the limit  $U \rightarrow \infty$  and  $J_H \rightarrow \infty$ , electronic motion at half-filling is suppressed due to single occupancy of the Mn sites; additional orbital splitting caused by superexchange interactions is left out.

The Hamiltonian  $\mathcal{H} = \mathcal{H}_{\text{JT}} + \mathcal{H}_{\text{L}}$  gives an orbitally ordered ground state:

$$|0, 0\rangle = \prod_{\ell} c_X^\dagger(\ell) \prod_{\ell'} c_Y^\dagger(\ell') |\{0\}\rangle, \quad (2)$$

where  $\{0\}$  refers to the lattice vibrational ground state with oxygen atoms in distorted equilibrium positions (Van Vleck  $Q_2$ -type distortions)  $u_{\ell \pm x} = \pm u_0$ ,  $u_{\ell \pm y} = \mp u_0$ ,  $u_{\ell \pm z} = 0$  if  $\ell \in A$  sublattice ( $\exp(i\vec{Q} \cdot \vec{\ell}) = 1$ ) and opposite sign distortions if  $\ell \in B$  sublattice ( $\exp(i\vec{Q} \cdot \vec{\ell}) = -1$ .) The magnitude of the distortion  $2u_0 = \sqrt{2\Delta/M\omega^2} = 0.296$  Å agrees with neutron diffraction data [3] within 10-15%, confirming the internal consistency of the model. Operators  $c_{X,Y}^\dagger$  create electrons with orbitals  $\Psi_{X,Y} = -(d_{3z^2-r^2} \mp d_{x^2-y^2})/\sqrt{2}$  alternating on  $A$  and  $B$  sublattices. The lowest-lying electronic excitation of the Hamiltonian (1) is a self-trapped exciton or orbiton [12], which gives a broad line in the optical conductivity [15] centered at  $2\Delta \approx 2$  eV.

In the  $n$ -phonon Raman process, incident light of frequency  $\omega_L$  is scattered with a shifted frequency  $\omega_S = \omega_L - n\omega$ . The Raman cross-section tensor  $\mathbf{R}^n$  can be found as following [17]:

$$\frac{\partial^2 \mathbf{R}^n}{\partial \omega_R \partial \Omega} = \frac{\sigma_0 \omega_S^2}{m_e^2 \omega_L^2} \left| \sum_{\{m\}, i} \frac{\langle 0, n | \hat{\varepsilon}_L \cdot \vec{p} | i, m \rangle \langle i, m | \hat{\varepsilon}_S \cdot \vec{p} | 0, 0 \rangle}{\Delta + N\{m\}\hbar\omega - \hbar\omega_L + i\gamma_m} + \text{NRT} \right|^2 \delta(\omega_R - n\omega) \quad (3)$$

where  $\sigma_0 = r_e^2$  is a Compton cross section ( $r_e = e^2/m_e c^2$ ). The summation goes over all electronic states  $i$  and all the corresponding vibrational quanta  $\{m\}$ .  $N\{m\} = m_x + m_y + m_z + m_{-x} + m_{-y} + m_{-z}$  is the total number of vibrational quanta. The nonresonant term (NRT) is obtained from the resonant term by permuting  $\hat{\varepsilon}_L$  with  $\hat{\varepsilon}_S$  and changing  $-\omega_L$  to  $\omega_S$ . The imaginary frequency  $\gamma_m$  takes into account the finite lifetime of the intermediate state  $|i, m\rangle$ . The final state  $|0, n\rangle$  has an electronic ground state plus  $n$  vibrational quanta. Summation over all the possible states with a total number of  $n$  vibrations is assumed in Eq. (3). For example, one phonon can be excited on any of the 6

neighboring oxygen atoms; two phonons can be excited in 21 ways; three phonons in 56 ways, and so on. The ground state couples to excited electronic states by the electron-radiation Hamiltonian ( $\vec{p} \cdot \vec{A}$ ). In LaMnO<sub>3</sub>, we consider only the lowest excited electronic state with an orbital flip (e.g.  $|X\rangle$ -type to  $|Y\rangle$ -type [11]). By neglecting coupling to higher electronic states we underestimate (perhaps by a significant factor) the first order Raman peak intensity. For multiphonon Raman scattering, in first approximation, we assume that only orbiton intermediate states contribute.

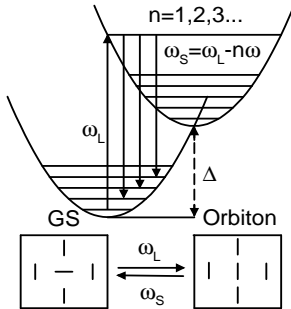


FIG. 1. Schematic Franck-Condon mechanism for the multiphonon Raman process via the orbiton intermediate state. The lowest energy configuration of the orbiton has energy  $\Delta$  and large oxygen distortions from the JT ground state (GS). The most probable intermediate state (the strongest resonance of the Raman process) occurs at  $\omega_L \approx 2\Delta \approx 2\text{eV}$ , rather than  $\omega_L = \Delta$ .

### III. LSDA DIPOLE MATRIX ELEMENTS

To evaluate dipole matrix elements in Eq. (3) we use the FC approximation. The wavefunctions  $|0, 0\rangle$ ,  $|i, m\rangle$  and  $|0, n\rangle$  are written as products of vibrational wavefunctions  $\chi(\vec{R})$  dependent on the oxygen positions  $\vec{R}$ , and electronic wavefunctions  $\psi(\vec{r}, \vec{R})$  dependent on both electronic  $\vec{r}$  and vibrational coordinates. The electronic dipole matrix element is a  $d$  to  $d$  transition and therefore forbidden when the surroundings are symmetric. Searching for a mechanism to activate this transition, we notice that an asymmetric oxygen displacement will cause Mn  $e_g$  orbitals to acquire an admixture of  $4p$  character. A typical mixing coefficient is

$$\gamma_z = \int d\vec{r} \psi_{3z^2-r^2} \frac{\partial V}{\partial u_z} \psi_z / (\epsilon_d - \epsilon_p) \quad (4)$$

where  $\psi_z$  is an orbital of  $p$  character, and  $\partial V / \partial u_z$  is the perturbation caused by a displacement of oxygen  $\ell + \hat{z}$  in  $\hat{z}$  direction. The corresponding allowed optical matrix element is

$$d_z = \int d\vec{r} \psi_{3z^2-r^2} p_z \psi_z. \quad (5)$$

The resulting dipole matrix element is

$$\langle i, m | \hat{\epsilon}_{S,L} \cdot \vec{p} | 0, n \rangle = \sum_{\alpha=x,y,z} \gamma_\alpha d_\alpha \epsilon_\alpha \langle m_x m_{-x} m_y m_{-y} m_z m_{-z} | (u_\alpha + u_{-\alpha}) | n_x n_{-x} n_y n_{-y} n_z n_{-z} \rangle \quad (6)$$

If the ground state is described by Eq. (2), then from symmetry one can show that  $\gamma_x d_x = \gamma_y d_y = -\gamma_z d_z / 2$ . In our previous work [12] a phenomenological parameter  $\gamma d = -\gamma_z d_z$  was introduced to account for the observed spectral weight of the optical conductivity peak due to the self-trapped exciton. The oscillator strength  $f$  defined as  $\int d\omega \sigma(\omega) = (\pi N e^2 / 2 m_e \Omega) f$  is equal in our model to  $f_{zz} = 2((\gamma d)^2 / m_e M \omega^2) / (2\Delta / \hbar \omega + 1)$ , and  $f_{xx} = f_{yy} = f_{zz} / 4$ . Here  $N / \Omega$  is the Mn atom concentration. The measured spectral weight  $540 \Omega^{-1} \text{cm}^{-1} \text{eV}$  of the lowest broad line centered at 2 eV [15] corresponds to  $f_{\text{exp}} = 0.113$  or  $\gamma d = 1.7$ . Here we use density functional theory (DFT) to calculate an induced dipole matrix elements to test whether our choice of the parameter  $\gamma d$  from the optical data was justified.

LaMnO<sub>3</sub> has been extensively studied by first-principles approaches [18] including the local-spin-density approximation (LSDA) of DFT, LDA+U, and Hartree-Fock methods. Information about electronic and magnetic structure, and about electron-phonon and Coulomb interactions has been obtained. Here we use LSDA to calculate the dipole matrix element for  $d$  to  $d$  transitions as it is induced by asymmetric oxygen distortions. Rather than calculating  $\partial V/\partial u_z$  and doing perturbation theory as in Eqs. (4,5), we directly calculate  $\langle i|\epsilon \cdot p|0 \rangle$  in the presence of an imposed asymmetric oxygen distortion.

To solve the LSDA equations we use the plane-wave pseudopotential method [19,20] with a spin-dependent exchange-correlation potential [21] and a supercell approach. Calculations were done for a 10-atom perovskite supercell with only  $Q_2$ -type JT oxygen distortions (the rotation of the MnO<sub>6</sub> octahedra is omitted.) The point group symmetry of the cell is thus  $D_{4h}$ . For convenience, the magnetic order is taken to be ferromagnetic with 4.00  $\mu_B$  spin magnetization per formula unit. The lattice constant 3.936 Å gives the same cell volume as observed for LaMnO<sub>3</sub>. The magnitude of the in-plane oxygen distortions along the Mn-O-Mn bonds is  $u_0 = 0.14$  Å. The self-consistent charge density was calculated using six special  $\mathbf{k}$  points in the irreducible wedge of the Brillouin zone. Then the self-consistent potential was used to calculate wavefunctions at the  $\Gamma$  point.

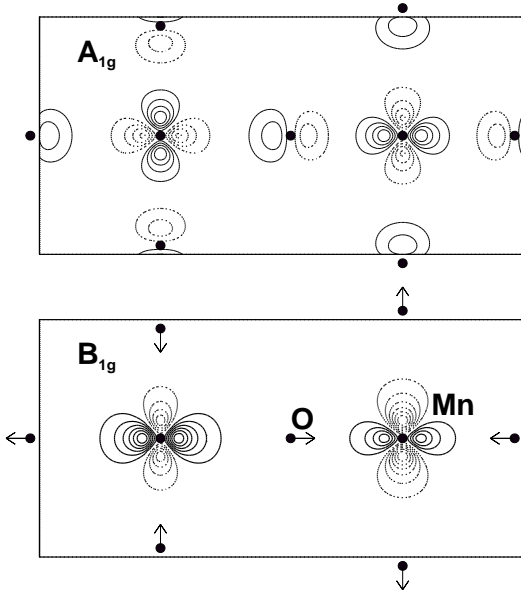


FIG. 2. The LSDA wavefunctions  $\Psi(\vec{r})$  at  $\vec{k} = (0, 0, 0)$  point for the Mn  $e_g$  states  $B_{1g}$  (occupied) and  $A_{1g}$  (empty). Arrows indicate the direction of the  $Q_2$ -type oxygen displacements in the  $xy$  plane. Negative (dashed) and positive (solid) contour values are in units of  $0.1 e^{1/2}/(a.u.)^{3/2}$

A symmetry analysis of the pseudowavefunctions for  $\mathbf{k} = (0, 0, 0)$  and plots of  $|\psi|^2$  around the Mn site allow us to distinguish Mn  $e_g$  states from other states. The  $e_g$  ( $X$ - and  $Y$ -type) orbitals form states of  $A_{1g}$  and  $B_{1g}$  symmetries. Two of the four Mn  $e_g$  states are shown on Fig. 2. By introducing a small displacement of all the apical oxygens in  $+\hat{z}$  direction along the Mn-O-Mn bonds, one induces a  $p_z$  dipole matrix element ( $A_{1g}$  to  $A_{1g}$  and  $B_{1g}$  to  $B_{1g}$ ). Similarly, in-plane oxygen displacement in the  $+\hat{x}$  direction induces a  $p_x$  matrix element. In table I we present LSDA results for these matrices. The imposed displacement has lowered the  $D_{4h}$  symmetry of the supercell, permitting transitions between states below and above the Fermi level which were previously labeled as  $A_{1g}$  and  $B_{1g}$ . The energies of the Mn  $e_g$  states do not alter much (less than 0.04 eV) for small distortions (0.016 Å) and the induced dipole matrix elements are linear with oxygen distortion.

It is convenient to measure the induced dipoles in units of  $(m_e M \omega^2)^{1/2} = 0.472 \hbar / (a_B)^2$ , where  $m_e$  and  $M$  are electron and oxygen masses and  $a_B$  is the Bohr radius. The calculated dipoles  $(\gamma d)_z = 2.39$  and  $(\gamma d)_{x,y} = 1.9$  give the oscillator strengths  $f_{zz} = 0.43$  and  $f_{xx,(yy)} = 0.27$ . These answers are somewhat larger than experiment, but well within the expected accuracy of our model. This accuracy is limited by four factors: (1) convergence of the LSDA result; (2) neglect of rotational distortions; (3) simplification of magnetic structure to ferromagnetic; and (4) applicability of LSDA to strongly-correlated electrons. We tested the first by varying the number of plane waves used in the pseudopotential expansion. The answers reported here used a plane-wave cut-off  $E_{pw} = 135$  Ry. The value of  $\gamma d$  increases by 9% at  $E_{pw} = 120$  Ry and decreases by 13% at  $E_{pw} = 100$  Ry, so the convergence error is estimated at 10%. Sources (2) and (3) will cause errors of similar size, we believe. The biggest uncertainty is source (4). In an

unrelated DFT study on the self-trapped-exciton in crystalline NaCl [22], we found evidence that LSDA incorrectly shifts the energy of localized states relative to delocalized states. However, the wavefunctions under consideration here are quite well-localized and agree qualitatively with expectation. Therefore we do not believe that point (4) is the source of a major error. Therefore we believe that this calculation provides firm evidence that phonon-activation is strong enough to account for the observation of  $d$  to  $d$  (orbital) transitions in optical reflectivity, as we assumed in our previous work, and as we now use to predict Raman spectra.

#### IV. THE RAMAN TENSOR

The absolute cross sections for the Raman process Eq. (3) can be evaluated using expression (6):

$$\frac{\partial^2 \mathcal{R}_{\alpha\beta}^n}{\partial \omega_R \partial \Omega} = \sigma_0 \frac{\omega_S^2}{\omega_L^2} (\gamma_\alpha d_\alpha \gamma_\beta d_\beta)^2 \delta(\omega_R - n\omega) \sum_{\{f\}} \delta(n - N\{f\}) \left| \sum_{m=0}^{\infty} \frac{\hbar\omega A_{\alpha\beta}(m, \{f\})}{\Delta + m\hbar\omega - \hbar\omega_L + i\gamma_m} + \text{NRT} \right|^2, \quad (7)$$

$$A_{\alpha\beta}(m, \{f\}) = \sum_{\{m'\}} \delta(m - N\{m'\}) \langle f | u_\alpha + u_{-\alpha} | m' \rangle \langle m' | u_\beta + u_{-\beta} | 0 \rangle \quad (8)$$

where the induced dipole matrix elements  $\gamma d$  and displacements  $u$  are measured in units of  $(m_e M \omega^2)^{1/2}$  and  $\sqrt{\hbar/M\omega}$  respectively. In order to evaluate vibrational overlap integrals  $A_{\alpha,\beta}(m, \{f\})$  one needs the expressions for overlap integrals of displaced harmonic oscillators,

$$\langle n_1 | n_2 \rangle = (-1)^{n_1 - n_2} \sqrt{n_1! n_2!} e^{-\kappa^2/2} \kappa^{n_1 - n_2} \sum_{k=0}^{n_2} (-1)^k \frac{\kappa^{2k}}{k!(n_2 - k)!(n_1 - n_2 + k)!}, \quad \text{if } n_1 \geq n_2 \quad (9)$$

$$\langle n_1 | u | n_2 \rangle = \frac{\kappa}{\sqrt{2}} \left( 1 + \frac{n_2 - n_1}{\kappa^2} \right) \langle n_1 | n_2 \rangle, \quad (10)$$

where  $\kappa$  is related to the Jahn-Teller gap as  $\Delta = 4\kappa^2 \hbar\omega$ . The overlap  $\langle n_1 | n_2 \rangle$  for  $n_1 < n_2$  has the same expression as (9) with  $n_1$  and  $n_2$  interchanged and the sign of the displacement  $u_0 = \sqrt{2}\kappa$  changed ( $\kappa \rightarrow -\kappa$ ). When using expressions (9, 10), the signs of the  $\ell + \hat{x}$ ,  $\ell - \hat{y}$  oxygens displacements are positive and  $\ell - \hat{x}$ ,  $\ell + \hat{y}$  are negative, if  $\ell \in A$  (reverse signs if  $\ell \in B$ ) and  $\ell \pm \hat{z}$  oxygens are undisplaced. Evaluation of the overlap integrals  $A_{\alpha\beta}(m, \{f\})$  is straightforward. For example, for the first order Raman peak, only four one-phonon final states will contribute:

$$A_{\alpha\beta}(m, \{f\} = 1 \dots 4) = \delta_{\alpha,\beta} \frac{e^{-\Delta} \Delta^m}{m!} \frac{m}{4\kappa\Delta} (\Delta + 1 - m) \quad (11)$$

with no contribution to the non-diagonal part of the tensor  $\alpha \neq \beta$ . For second- and third-order Raman scattering, four and eight final states contribute to the non-diagonal part of the tensor:

$$\begin{aligned} A_{xy(yz, zx)}(m, \{f\} = 1 \dots 4) &= \pm \frac{e^{-\Delta} \Delta^m}{m!} \frac{m}{2\Delta}, \\ A_{xy(yz, zx)}(m, \{f\} = 1 \dots 8) &= \pm \frac{e^{-\Delta} \Delta^m}{m!} \frac{\kappa m}{\sqrt{2}\Delta^2} (\Delta + 1 - m) \end{aligned} \quad (12)$$

The formulas for the diagonal parts of the higher-order Raman tensors are more complicated and will not be given here.

To model the damping term  $\gamma_m$  of vibrational level  $m$ , we use expression  $\gamma_m = \gamma_0 \sqrt{m+1}$ , as in a sequence of convolved Gaussians, intended to mimic the local densities of phonon states on oxygen atoms. The value  $\gamma_0 = 120 \text{ cm}^{-1}$  was taken. The Raman cross section shown on Fig. 3 has a pronounced resonant behavior when the laser frequency  $\omega_L$  approaches the orbital energy  $2\Delta$ . The first-order cross-section as seen in Fig. 3 is underestimated, because we neglected coupling to higher electronic levels in Eq. (7), whose contribution to multiphonon peaks is probably negligible. The polarization dependence of the cross-section is only due to the dipole matrix element effect, namely  $\mathcal{R}_{xx}^{1,2,3} = \mathcal{R}_{yy}^{1,2,3} = \mathcal{R}_{zz}^{1,2,3}/16$ ,  $R^{2,3,yz} = R_{zx}^{2,3} = 4R_{xy}^{2,3}$ . The anisotropy of the optical conductivity  $\sigma_{xx}/\sigma_{zz}$  is quadratic and Raman intensity  $\mathcal{R}_{xx}/\mathcal{R}_{zz}$  fourth-power in the dipole matrix-element anisotropy  $\gamma_x d_x / \gamma_z d_z$ . Actual occupied  $e_g$  orbitals may be rotations of our idealized state Eq. (2) in the  $e_g$  space. Even small deviations from Eq. (2) might cause a noticeable change of the ratio  $\gamma_x d_x / \gamma_z d_z$  from the value 0.5. Therefore the predicted anisotropies

of 4 and 16 for optical and Raman spectra are not necessarily robust, but the relation  $\mathcal{R}_{xx}/\mathcal{R}_{zz} = (\sigma_{xx}/\sigma_{zz})^2$  should hold.

Published Raman measurements [16] on undoped LaMnO<sub>3</sub> do not extend to the multiphonon region and resonant behavior has not been tested experimentally. Most experiments use the Ar<sup>+</sup> laser, for which frequency  $\omega_L = 2.41$  eV, we predict the multiphonon cross sections  $\mathcal{R}_{zz}^2 = 0.514$ ,  $\mathcal{R}_{zz}^3 = 0.243$ ,  $\mathcal{R}_{yz}^2 = 0.056$ ,  $\mathcal{R}_{yz}^3 = 0.025$  in units of  $\sigma_0$  sr<sup>-1</sup>. Recently some features in Raman spectra on LaMnO<sub>3</sub> around 1100 cm<sup>-1</sup> were reported by several groups [23,24]. These are probably the effect we are predicting.

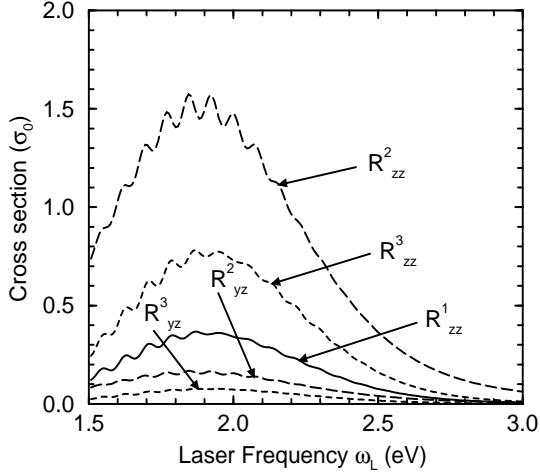


FIG. 3. The absolute value of the multiphonon Raman cross section per solid angle versus incident photon energy. Resonant behavior is predicted for  $\omega_L$  close to orbiton energy  $2\Delta = 1.9$  eV. The damping constant is  $\gamma_0 = 120$  cm<sup>-1</sup>, the induced dipoles are  $-\gamma_z d_z = 2\gamma_x d_x = 1.7 (m_e M \omega^2)^{1/2}$ , cross section unit is  $\sigma_0 = (e^2/m_e c^2)^2$ .

## V. CONCLUSION

We advocate a picture of the orbitally ordered state of LaMnO<sub>3</sub> where electron-phonon interactions (in a context of large Hund and Hubbard energies) have a major influence. Our picture is disputed by other theorists [25]. Therefore we attempt here to provide predictions which can qualitatively distinguish our model from others. In our model, the lowest electronic excitation is the 1.9 eV transition across the Jahn-Teller gap, modified by self-trapping to give a minimum gap half as large. This has successfully described the observed [15] optical gap as a Franck-Condon broadened self-trapped exciton. The present paper uses density-functional theory to eliminate the need for a phenomenological coupling  $\gamma d$  to account for this transition.

As a more stringent test, we here predict a new feature unique to the FC physics of the self-trapped exciton, namely a sequence of resonant multiphonon Raman peaks. We predict the absolute values of the multiphonon Raman cross section tensors.

A hot luminescence process can also give rise to a multiphonon peaks. Incident light can excite an orbiton with a long lifetime which can recombine after vibrational energy  $n\omega$  being lost in the intermediate state through anharmonic interaction. The question whether the Raman or hot luminescence mechanisms dominate the scattering intensity has an old history [26]. In the Raman case the intensity of the higher order peaks should decrease and the width of the peak representing a convolved density of local phonon modes should increase. In the hot luminescence the intensities of the higher order peaks are of the same order and the width of the lines decrease with increasing order. In addition a strong emission peak can be observed at the exciton absorption edge. Raman techniques can serve as a direct probe of the orbiton excitation in LaMnO<sub>3</sub>.

## ACKNOWLEDGMENTS

We thank D. Romero for encouragement on this problem, A. J. Millis for nudging us to do DFT calculations, and M. Weinert for valuable discussions of the DFT results. This work was supported in part by NSF Grant No. DMR-0089492.

- 
- [1] *Colossal Magnetoresistance, Charge Ordering, and Related Properties of Manganese Oxides*, edited by C.N.R. Rao and B. Raveau (World Scientific, Singapore, 1998); *Physics of Manganites*, edited by T. A. Kaplan and S. D. Mahanti (Kluwer Academic, New York, 1999); *Colossal Magnetoresistive Oxides*, edited by Y. Tokura (Gordon & Breach, New York, 2000).
- [2] R. M. Kusters, J. Singelton, D. A. Keen, R. McGreevy, and W. Hayes, *Physica B* **155**, 362 (1989); S. Jin, T. H. Tiefel, M. McCormack, R. A. Fastnacht, R. Ramesh, and L. H. Chen, *Science* **264**, 413 (1994); J. M. D. Coey, M. Viret, and S. von Molnar, *Adv. Phys.* **48**, 167 (1999).
- [3] J. Rodriguez-Carvajal, M. Hennion, F. Moussa, A. H. Moudden, L. Pinsard and A. Revcolevschi, *Phys. Rev. B* **57**, 3189 (1998); T. Proffen, R. G. DiFrancesco, S. J. L. Billinge, E. L. Brosha and G. H. Kwei, *Phys. Rev. B* **60**, 9973 (1999).
- [4] Y. Murakami, J. P. Hill, D. Gibbs, M. Blume, I. Koyama, M. Tanaka, H. Kawata, T. Arima, Y. Tokura, K. Hirota, and Y. Endoh, *Phys. Rev. Lett.* **81**, 582 (1998).
- [5] F. Moussa, M. Hennion, J. Rodriguez-Carvajal, H. Moudden, L. Pinsard, and A. Revcolevschi, *Phys. Rev. B* **54**, 15149 (1996); K. Hirota, N. Kaneko, A. Nishizawa, and Y. Endoh, *J. Phys. Soc. Jpn.* **65**, 3736 (1996).
- [6] K. I. Kugel and D. I. Khomskii, *Sov. Phys. Usp.* **25**, 231 (1982).
- [7] Y. Tokura and N. Nagaosa, *Science* **288**, 462 (2000).
- [8] A. J. Millis, P. B. Littlewood, and B. I. Shraiman, *Phys. Rev. Lett.* **74**, 5144 (1995); A. J. Millis, B. I. Shraiman, and R. Mueller, *Phys. Rev. Lett.* **77**, 175 (1996).
- [9] J. Kanamori, *J. Appl. Phys.* **31**, 14S (1960).
- [10] T. Hotta, A. L. Malvezzi, and E. Dagotto, *Phys. Rev. B* **62**, 9432 (2000).
- [11] P. B. Allen and V. Perebeinos, *Phys. Rev. B* **60**, 10747 (1999).
- [12] P. B. Allen and V. Perebeinos, *Phys. Rev. Lett.* **83**, 4828 (1999).
- [13] L. L. Krushinskii and P. P. Shorygin, *Optics and Spectroscopy* **11**, 12 (1961); A. C. Albrecht, *J. Chem. Phys.* **34**, 1476 (1961); E. Mulazzi, *Phys. Rev. Lett.* **25**, 228 (1970). P. P. Shorygin, *Sov. Phys. – Usp.* **16**, 99 (1973).
- [14] A. J. Millis, *Phys. Rev. B* **53**, 8434 (1996).
- [15] J. H. Jung, K. H. Kim, D. J. Eom, T. W. Noh, E. J. Choi, J. Yu, Y. S. Kwon, and Y. Chung, *Phys. Rev. B* **55**, 15489 (1997); J. H. Jung, K. H. Kim, T. W. Noh, E. J. Choi, and J. Yu, *Phys. Rev. B* **57**, 11043 (1998).
- [16] M. N. Iliev, M. V. Abrashev, H.-G. Lee, V. N. Popov, Y. Y. Sun, C. Thomsen, R. L. Meng, and C. W. Chu, *Phys. Rev. B* **57**, 2872 (1998); V. B. Podobedov, A. Weber, D. Romero, J. P. Rice and H. D. Drew, *Phys. Rev. B* **58**, 43 (1998); E. Granado, J. A. Sanjurjo, C. Rettori, J. J. Neumeier and S. B. Oseroff, *Phys. Rev. B* **62**, 11304 (2000).
- [17] M. Cardona, in *Light Scattering in Solids II*, edited by M. Cardona and G. Güntherodt (Topics in Applied Physics **50**, Springer, Berlin 1982) p. 19.
- [18] D. D. Sarma, N. Shanthi, S. R. Barman, N. Hamada, H. Sawada and K. Terakura, *Phys. Rev. Lett.* **75**, 1126 (1995); W. E. Pickett and D. Singh, *Phys. Rev. B* **53**, 1146 (1996); S. Satpathy, Z. S. Popović and F. R. Vukajlović, *Phys. Rev. Lett.* **76**, 960 (1996); I. Solovyev, N. Hamada and K. Terakura, *Phys. Rev. Lett.* **76**, 4825 (1996); *Phys. Rev. B* **53**, 7158 (1996); D. J. Singh and W. E. Pickett, *Phys. Rev. B* **57**, 88 (1998); Y.-S. Su, T. A. Kaplan, S. D. Mahanti and J. F. Harrison, *Phys. Rev. B* **61**, 1324 (2000).
- [19] N. Chetty, M. Weinert, T. S. Rahman, and J. W. Davenport, *Phys. Rev. B* **52**, 6313 (1995).
- [20] To generate pseudopotentials [N. Troullier and J. L. Martins, *Phys. Rev. B* **43**, 1993 (1991)] we use core radii 1.6, 1.6, 3.2 a. u. for O  $2s^2$ ,  $2p^{3.5}$ ,  $3d^{0.5}$  orbitals; 2.5, 3.0, 1.3 a. u. for Mn  $4s^{1.5}$ ,  $4p^{0.5}$ ,  $3d^5$  orbitals; and 3.9, 4.5, 2.2 a. u. for La  $6s^{1.5}$ ,  $6p^{0.5}$ ,  $5d^1$  orbitals with a nonlinear core correction for Mn and La. Plane wave cutoffs were  $E_{pw}=135$  Ry for the wave functions and 130 Ry for the pseudopotential truncation [M. Alatalo, M. Weinert and R. E. Watson, *Phys. Rev. B* **60**, 7680 (1999)].
- [21] D. M. Ceperley and B. J. Adler, *Phys. Rev. Lett.* **45**, 566 (1980).
- [22] V. Perebeinos, P. B. Allen and M. Weinert, *Phys. Rev. B* **62**, 12589 (2000).
- [23] P. Björnsson, M. Rübhausen, J. Bäckström, M. Käll, S. Eriksson, J. Eriksen, and L. Börjesson, *Phys. Rev. B* **61**, 1193 (2000).
- [24] D. B. Romero, V. B. Podobedov, A. Weber, J. F. Mitchell, Y. Moritomo, and H. D. Drew, preprint.
- [25] J. Brink, P. Horsch, and A. M. Oleś, *Phys. Rev. Lett.* **85** 5174 (2000); V. Perebeinos and P. B. Allen, **85** 5178 (2000);
- [26] E. F. Gross, S. A. Ppermogorov, V. V. Travnikov, and A. V. Sel'kin, *Fiz. Tverd. Tela* **13**, 699 (1971) [*Sov. Phys.-Solid State* **13**, 578 (1971)]; M. V. Klein, *Phys. Rev. B* **8**, 919 (1973); Y. R. Shen, *Phys. Rev. B* **9**, 622 (1974); T. P. Martin, *Phys. Rev.* **13**, 3618 (1976).

TABLE I. The absolute values of the induced dipole matrix elements  $p_z$  (left) and  $p_x$  (right) per unit oxygen displacements in units of  $(m_e M \omega^2)^{1/2}$  between the LSDA wavefunctions of the  $A_{1g}$  and  $B_{1g}$  symmetry before an additional asymmetric oxygen distortion. The resulting oscillator strengths for the transition between the occupied (*occ*) and empty (*em*) states are  $f_{zz} = 0.43$  and  $f_{xx,(yy)} = 0.27$ , which corresponds to  $(\gamma d)_z = 2.39$  and  $(\gamma d)_{x,y} = 1.9$ .

	$A_{1g}^{occ}$	$A_{1g}^{em}$	$B_{1g}^{occ}$	$B_{1g}^{em}$	$A_{1g}^{occ}$	$A_{1g}^{em}$	$B_{1g}^{occ}$	$B_{1g}^{em}$
$A_{1g}^{occ}$	0	3.37	0	0	0	1.83	2.03	0.90
$A_{1g}^{em}$	3.37	0	0	0	1.83	0	1.55	0.05
$B_{1g}^{occ}$	0	0	0	0.17	2.03	1.55	0	0.82
$B_{1g}^{em}$	0	0	0.17	0	0.90	0.05	0.82	0